

RESEARCH ARTICLE

10.1002/2017JA024009

Key Points:

- Brazilian (dayside) equatorial ionospheric response is dominated by two strong PPEF phases even under background disturbance dynamo effects
- Vertical expansion of equatorial F layer and formation of F_3 layer is consistently observed during both the PPEF phases
- Strong equatorial super fountain process rejuvenated by PPEF caused the poleward departure of EIA crest to $\sim 40^\circ\text{S}$ latitude

Supporting Information:

- Supporting Information S1
- Movie S1
- Movie S2

Correspondence to:

K. Venkatesh,
venkatkau@gmail.com

Citation:

Venkatesh, K., S. Tulasi Ram, P. R. Fagundes, G. K. Seemala, and I. S. Batista (2017), Electrodynamic disturbances in the Brazilian equatorial and low-latitude ionosphere on St. Patrick's Day storm of 17 March 2015, *J. Geophys. Res. Space Physics*, 122, 4553–4570, doi:10.1002/2017JA024009.

Received 7 FEB 2017

Accepted 23 MAR 2017

Accepted article online 28 MAR 2017

Published online 12 APR 2017

Electrodynamic disturbances in the Brazilian equatorial and low-latitude ionosphere on St. Patrick's Day storm of 17 March 2015

K. Venkatesh¹ , S. Tulasi Ram², P. R. Fagundes¹ , Gopi K. Seemala² , and I. S. Batista³ 

¹IP&D, Universidade do Vale do Paraíba, São Paulo, Brazil, ²Indian Institute of Geomagnetism, Navi Mumbai, India, ³Instituto Nacional de Pesquisas Espaciais, São Paulo, Brazil

Abstract The St. Patrick's Day storm of 17 March 2015 has a long-lasting main phase with the Dst reaching a minimum of -223 nT. During the main phase, two strong prompt penetration electric field (PPEF) phases took place; first with the southward turning of IMF B_z around ~ 1200 UT and the second with the onset of a substorm around ~ 1725 UT leading to strong equatorial zonal electric field enhancements. The consequent spatiotemporal disturbances in the ionospheric total electron content and the resultant modifications in the equatorial ionization anomaly (EIA) over the Brazilian longitudinal sector are investigated in detail. The simultaneous measurements from a large network of GPS receivers, ionosonde, and magnetometers over the Brazilian longitudinal sector are used for this study. In the presence of enhanced zonal electric field, the equatorial F_2 layer peak ($h_m F_2$) experienced a rapid uplift without any significant change in the base height ($h'F$); while the F_2 layer is redistributed into F_2 and F_3 layers. The enhanced zonal electric field due to PPEF led to the strong super fountain effect under which the anomaly crest departed poleward to $\sim 40^\circ\text{S}$ latitude. In the presence of westward and equatorward wind surge over Brazil with the coexisting disturbance dynamo fields, strong hemispheric asymmetry is seen in the storm time response of EIA during both the PPEF phases.

1. Introduction

The energetic events on the Sun and consequent effects on the Earth's magnetosphere and upper atmosphere including ionosphere comprise space weather. One of the important phenomena in space weather is the geomagnetic storms caused by enhanced solar wind energy input associated with solar coronal mass ejections (CME), coronal holes-high speed streams, and associated corotating interaction regions (CIRs). Studies on the ionospheric response to the geomagnetic storms have gained extensive importance because of the complex nature of the solar wind-magnetosphere-ionosphere coupling through magnetic reconnection [Wolf, 1975; Tsurutani and Gonzalez, 1997; Somayajulu, 1998] and also due to the distinctness in the characteristics of each individual storm.

During the geomagnetic storms, the equatorial zonal electric field, which is usually eastward in dayside and westward in nightside experience several changes leading to severe modifications in the equatorial electrodynamic processes. The storm time perturbations in the zonal electric field occur mainly due to two important processes, namely, (1) the prompt penetration electric fields (PPEF) and (2) the disturbance dynamo electric fields (DDEF). During the geomagnetic storms, the dynamic reconnection between solar wind and Earth's magnetosphere results in the high-latitude electric fields through field aligned currents. These electric fields promptly penetrate into the equatorial latitudes through Earth-ionosphere waveguide [Nishida, 1968; Kikuchi et al., 1996, 2000; Gonzales et al., 1979], and it was first modeled by Vasylunas [1970]. The PPEF causes perturbations in the zonal electric field for shorter durations of about 30 min to 2 h and occur almost instantaneously with the southward (undershielding electric field) or northward (overshielding electric field) turning of the interplanetary magnetic field [Senior and Blanc, 1984; Kelley et al., 2003]. When there is a southward turning of the IMF B_z , the enhanced convection electric fields results in PPEF which are oriented dawn to dusk, i.e., eastward on the dayside and westward on the nightside similar to that of quiet time zonal electric field [Nishida, 1968; Kikuchi et al., 1996]. During northward turning of IMF B_z , the overshielding electric fields causes perturbations which are westward on the dayside and eastward on the nightside [Rastogi and Patel, 1975; Kelley et al., 1979; Kikuchi et al., 2000; Fejer, 2002].

On the other hand, the energy deposited in the upper atmosphere over high latitudes and the associated Joule and particle heating results in the global variations of the thermospheric wind system. This produces

disturbance dynamo electric fields (DDEFs) which were first predicted by *Blanc and Richmond* [1980]. Later, *Fejer et al.* [1983] identified the disturbance dynamo electric fields for the first time using the incoherent scatter radar measurements over Jicamarca. The DDEFs effects at low latitudes appear few hours after the energy input at high latitudes and often become dominant during the later phase of the storm with nonuniform time delays at different latitudes and lasts for few hours to more than a day [*Richmond et al.*, 2003]. At the equatorial latitudes the dynamo electric fields are directed westward during daytime and eastward during nighttime [*Scherliess and Fejer*, 1997].

It is known that, during quiet time itself, the equatorial and low-latitude ionosphere exhibit significant spatiotemporal variability being characterized by typical electrodynamic phenomenon such as the equatorial electrojet (EEJ), equatorial ionization anomaly (EIA), equatorial spread-F (ESF), and plasma bubbles (EPBs). During the disturbed geomagnetic conditions, the storm time perturbations in the zonal electric field due to PPEFs and DDEFs cause severe modifications to equatorial electrodynamic processes leading to more complex variability of equatorial and low-latitude ionosphere (see excellent review by *Sastri et al.* [2003a] and *Tulasi Ram et al.* [2008]). The ionospheric electron density is mainly found to be either enhanced or depleted during the geomagnetic storms which are known as positive or negative ionospheric storms, respectively [*Prölss*, 1995; *Förster and Jakowski*, 2000; *Mendillo*, 2006; *Balan et al.*, 2012 and *Danilov*, 2013]. For the positive storm occurrence, increase in the O/N₂ ratio, storm time thermospheric winds, PPEFs, and DDEFs as well as the plasmaspheric downward fluxes are known to be the main sources [*Rishbeth*, 1991; *Fuller-Rowell et al.*, 1996; *Richmond and Lu*, 2000; *Huang et al.*, 2005; *Crowley et al.*, 2008; *Danilov*, 2013]. The storm time decrease in the O/N₂ ratio leading to the enhancement of ion loss rate is reported to be the primary cause for the negative storm occurrence [*Rishbeth*, 1991; *Fuller-Rowell et al.*, 1994; *Prölss*, 1995; *Field and Rishbeth*, 1997].

The recent geomagnetic storm that occurred on the St. Patrick's Day of 17 March 2015 is the strongest storm in the 24th solar cycle with the minimum *Dst* of -223 nT while the *AE* crossed 2000 nT with the highest recorded *Kp* value of 8. Several investigations have been carried out from different regions to understand the influence of this severe geomagnetic storm on the ionospheric behavior [*Astafyeva et al.*, 2015; *Tulasi Ram et al.*, 2015; *Fagundes et al.*, 2016; *Nava et al.*, 2016, *Huang et al.*, 2016, etc.]. *Astafyeva et al.* [2015] studied the response of the ionospheric electron content and hemispheric asymmetry using the GPS and satellite measurements. The response of equatorial zonal electric field to PPEF from dusk to premidnight sector during this storm have been investigated by *Tulasi Ram et al.* [2015] using the ionosonde and satellite measurements over Southeast Asian region. Using the measurements of DMSP satellites, *Huang et al.* [2016] studied the characteristics of DDEFs in the topside ionosphere. *Nava et al.* [2016] studied the ionospheric response to this storm in the Asian, African, and American sectors using the global total electron content (GEC) and regional total electron content (REC) variations. *Kuai et al.* [2016] compared the effect of this storm in different regions and noted that distinct features are seen in the American sector. The positive and negative ionospheric storm effects in the Brazilian sector during main and recovery phases, respectively, were reported by *Fagundes et al.* [2016]. In the context of the severity of this St. Patrick's Day storm, and also due to the distinct features noted in the American region which is on the dayside hemisphere during the main phase of the storm, the present study is focused to investigate in detail the storm induced daytime zonal electric field perturbations and their influence on the spatiotemporal characteristics of the ionosphere using simultaneous observations from Brazilian longitudinal sector. In the present study, the simultaneous observations from GPS, ionosonde, and magnetometers over the Brazilian longitudes along with the total electron content (TEC) from North and South American sectors available from the Madrigal database are used. The EEJ variations along with the ionosonde observations over equator in the Brazilian sector are used to study the convective electric field influence on the daytime zonal electric field and consequence response of the equatorial ionospheric *F* layer. Further, the TEC observations from a large network of 120 GPS receivers all over Brazil along with the TEC data over North and South American sectors from Madrigal database are used to investigate the spatiotemporal electron density disturbances over Brazilian sector and the responsible physical mechanisms in terms of PPEFs associated with substorm and resultant equatorial super fountain effects. In the following, the different data sets used in the present study are briefly described in section 2. The occurrence of two PPEF phases and resultant electrodynamic disturbances observed over Brazilian equatorial and low-latitude regions are presented in section 3. The responsible physical mechanisms are discussed in section 4, and the important findings are summarized in section 5.

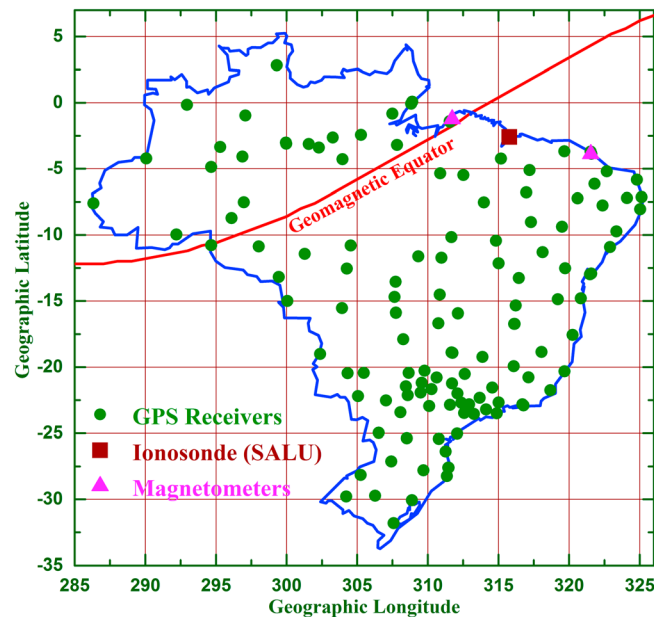


Figure 1. Brazilian map showing the geographical locations of Instituto Brasileiro de Geografia e Estatística (IBGE) network of 120 GPS receivers, magnetometers (magenta colored triangles) and ionosonde at Sao Luis (brown colored square). The red colored curve is the geomagnetic equator.

to study the latitudinal and interhemispheric response of EIA to the storm-induced electric fields, the TEC data in the Northern and Southern Hemispheres along the Brazilian longitudes are considered from the Madrigal database (<http://madrigal.haystack.mit.edu/madrigal/>). The red colored curve in this figure shows the geomagnetic equator over Brazil which has a typical inclined structure with reference to the geographic equator and makes it more interesting to investigate the equatorial electrodynamic characteristics over Brazil when compared to the other longitudinal sectors over the globe.

Further, to understand the equatorial *F* layer behavior during the storm, the digisonde measurements are analyzed from an equatorial station Sao Luis (SALU, 2.6°S, 315.8°E and 3.37° S dip latitude) and its location is shown as a brown colored square in Figure 1. The digisonde data over SALU is downloaded from the UML Digital Ionogram Database (DID Base: <http://ulcar.uml.edu/DIDBase/>; <http://spase.info/SMWG/Observatory/GIRO>) [Reinisch and Galkin, 2011]. All the ionograms are manually scaled to derive different *F* layer parameters. To study the zonal electric field characteristics and its response to storm induced convective fields, the magnetometer measurements over an equatorial station Belem (1.24°S, 311.73°E and -0.07 dip latitude) and an off-equatorial station Eusebio (3.88°S, 321.54°E and -7.63° dip latitude) are analyzed. The locations of these two magnetometers are shown as magenta colored triangles in Figure 1. The magnetometer data over Belem are downloaded from the AMBER magnetometer network [Yizengaw and Moldwin, 2009] being operated by the Boston college and funded by NASA and AFOSR. The magnetometer measurements over Eusebio are from the EMBRACE network [Denardini et al., 2013] operated by the Instituto Nacional de Pesquisas Espaciais (INPE), Brazil. The *H* component values of the Earth magnetic field at the equatorial and off-equatorial locations are normalized to the difference between the *H*-component values and the mean midnight values for the five quietest days. The quiet days are considered from the World Data Centre (WDC) for Geomagnetism, Kyoto (<http://wdc.kugi.kyoto-u.ac.jp/qddays/index.html>). Further, the equatorial electrojet strength values are estimated by calculating the difference between the ΔH values at equatorial and off equatorial stations. The disturbance storm time index (*Dst*) values are obtained from the WDC, Kyoto (<http://wdc.kugi.kyoto-u.ac.jp/dstdir/index.html>). The geomagnetic indices (IMF *Bz*, *SYM-H*, *AE*, *AL*, and *AU*) with 1 min time resolution, interplanetary electric field (IEFy) and the *Kp* index value averaged at every 3 h are taken from the Space Physics Data Facility (SPDF) at http://omniweb.gsfc.nasa.gov/ow_min.html. The solar wind parameters time shifted to bows shock nose are also obtained from the SPDF website (http://omniweb.gsfc.nasa.gov/form/sc_merge_min1.html). Further, to identify the possible presence of substorms, the wave power index (*Wp*) which is related to wave power of low-latitude Pi2 pulsations is obtained from the website (<http://s-cubed.info/data/index.html>).

2. Database

The spatiotemporal disturbances in the ionospheric electron content observed over the Brazilian equatorial and low-latitude sectors during the St. Patrick's Day storm of 17 March 2015 are investigated in detail using observations from GPS, ionosonde, and magnetometers. Figure 1 shows the Brazilian map along with the locations (green dots) of the large network of 120 GPS receivers spanning all over Brazil for more than 35° × 35° geographical extent in latitude and longitudes. The GPS receiver network over Brazil is deployed and maintained by the Instituto Brasileiro de Geografia e Estatística (IBGE). The dual-frequency measurements at L1 and L2 from all these GPS receivers are analyzed to compute the TEC values using the differential delay technique [Seemala and Valladeres, 2011]. Also, to study the latitudinal and interhemispheric response

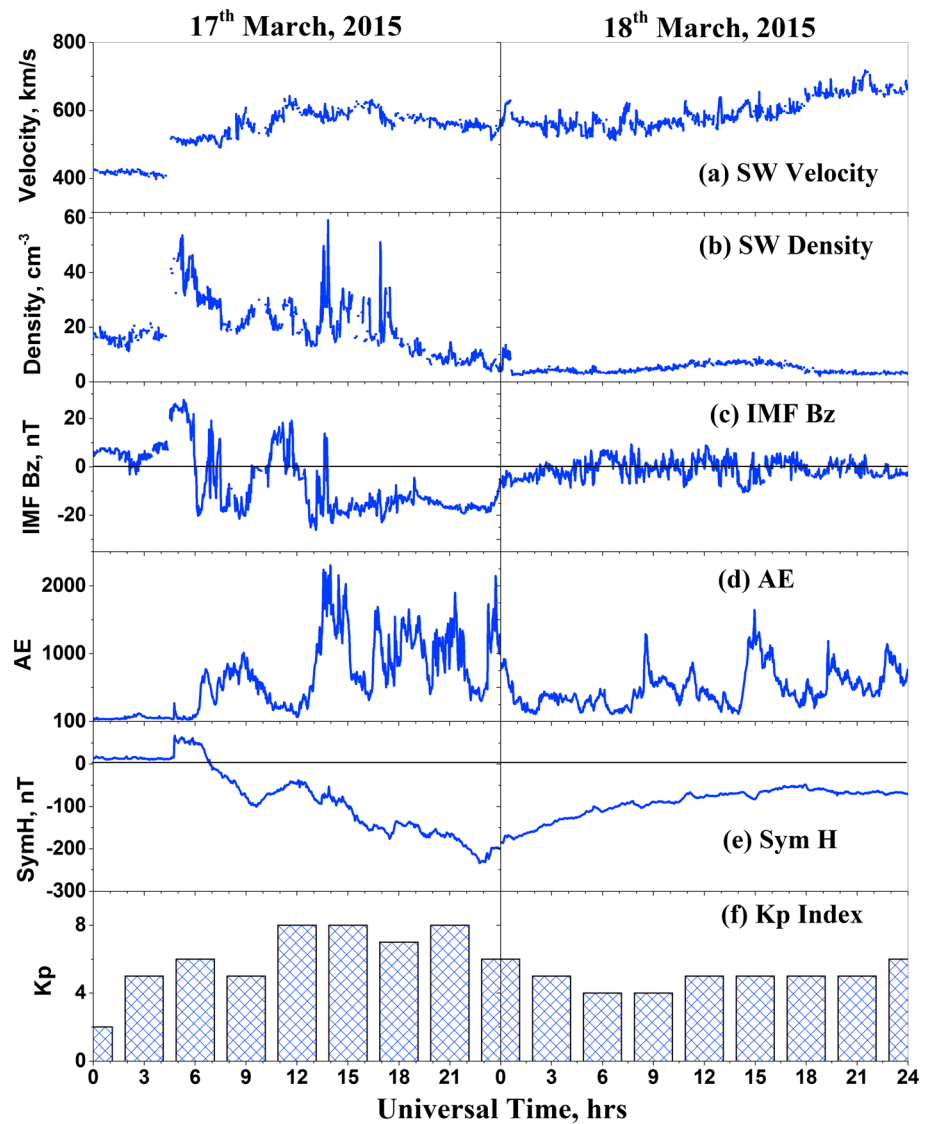


Figure 2. The diurnal variations of (a) solar wind velocity, (b) solar wind density, (c) IMF Bz, (d) AE, (e) SYM-H, and (f) Kp index during the main and recovery phase of the St. Patrick’s Day storm on 17 and 18 March 2015.

3. Results

In connection with the C-9 class solar flare from Sunspot AR2297, a coronal mass ejection (CME) erupted on 15 March 2015 between 0045 UT and 0200 UT. The CME has hit the earth’s magnetosphere at 0445 UT on 17 March 2015 (<http://www.spaceweather.com>) resulting in the 24th solar cycle’s strongest geomagnetic storm so far, the St. Patrick’s Day storm. The temporal variations of solar wind and geomagnetic parameters during 17 and 18 March 2015 are presented in Figure 2. It is observed that the solar wind velocity (Figure 2a) and solar wind density (Figure 2b) shows an enhancement around 0430 UT on 17 March 2015 following the arrival of CME shock. The sudden commencement of the storm occurred around 0445 UT as the z component of the interplanetary magnetic field (IMF Bz; Figure 2c) is initially northward and the SYM-H (Figure 2e) shows a sharp rise by 0448 UT marking the initial phase of storm. The first southward turning of IMF Bz is noticed around 0600 UT, and at the same time SYM-H started decreasing, representing the main phase onset of the storm. Initially, the IMF Bz shows short-lived positive values, and later it remained southward until 0930 UT while the SYM-H reached -97 nT. Afterward, the IMF Bz turned northward around 1024 UT and stayed northward for few hours and again turned southward around 1200 UT. Later the IMF Bz is constantly southward for a longer duration up to 2300 UT resulting in the magnetic reconnection and enhanced ring current.

In the presence of long-lasting southward IMF Bz, the *SYM-H* reached to a minimum value of -232 nT. Around 2300 UT, the IMF Bz started increasing leading to the recovery phase of the storm which lasted for few days [Spogli *et al.*, 2016]. The Auroral Electrojet (*AE*) index presented in Figure 2d shows an increase to a maximum of 1000 nT around 9 UT during the first southward phase of IMF Bz. Later around 1200 UT, the *AE* exhibits a rapid increase to a maximum of 2000 nT followed by several fluctuations during the main and recovery phases of the storm. The increased SW velocity remains high during the main and recover phases of the storm. The solar wind density shows higher values during the complete main phase of the storm and came to the normal level during the recovery phase of the storm. The 3 h averaged *Kp* index presented in Figure 2f shows maximum value of 8 during the main phase, and it vary around 5 during the recovery phase.

As it is mentioned before, during the southward and northward turning of IMF Bz, the zonal electric field gets severely perturbed resulting in significant disturbances in the equatorial electrodynamic and consequently, the electron density distribution over the equatorial and low latitudes exhibits large deviations when compared to the quiet time behavior. During the main phase of the storm, the Brazilian sector is on the dayside giving an opportunity to investigate the response of the equatorial electrojet to the storm-induced electric fields and to understand the consequent influence on the daytime electrodynamic phenomena such as the EIA during this strong geomagnetic storm.

To study the electric field response during the main phase of the storm, the variations of interplanetary electric field (IEFy) from 1000 to 2000 UT on 17 March 2015 are presented in Figure 3a. It is seen from this figure that the interplanetary electric field is mostly negative between 1000 and 1200 UT during which the IMF Bz was northward (Figure 2c). It is also observed from Figure 2c that the IMF Bz turned southward at ~ 1200 UT followed by a rapid and strong negative excursion at 1240 UT. As a result, the IEFy presented in Figure 3a shows that the interplanetary electric field turns positive around 1200 UT, and later it exhibits a rapid rise at 1240 UT. Simultaneous variations of *AE*, *AL*, and *AU* are presented as green, dark yellow, and magenta curves, respectively, in Figure 3b. It can be observed that the *AE* (*AL*) started increasing (decreasing) gradually from ~ 1200 UT. The rapid rise (fall) in *AE* (*AL*) indicates the onset of a storm time substorm. Hence, to identify the possible presence of any substorms during the storm main phase, the variation of wave power index (*Wp* index) is presented in Figure 3c. A number of previous studies have shown that the wave power of low-latitude Pi2 pulsations has close relation to the substorm onset which can be identified by a prompt increase of the *Wp* index [Nosé *et al.*, 2009, 2012]. It is observed from Figures 3b and 3c that the *AE* (*AL*) exhibits sudden increase (decrease), and simultaneously, *Wp* index show a sharp peak at 1330 UT clearly indicating the onset of a substorm at 1330 UT on 17 March 2015. The occurrence of substorm at 1330 UT and its influence on the dusk sector (Indian-Thailand-Vietnam regions) are reported earlier by Tulası Ram *et al.* [2015]. The effect of substorm at 1330 UT on the formation of ionospheric irregularities over Southeast Asian sector is reported by Spogli *et al.* [2016]. In order to further study the zonal electric field response in the dayside, the EEJ variations in the Brazilian sector are presented in Figure 3d (red colored curve) along with the quiet time variations (blue colored curve). It is seen from this figure that the zonal electric field is negative and westward in the morning hours till ~ 1200 UT after which the electric field turned eastward and become positive. It can be noticed that around 1240 UT, simultaneously with a rapid rise in the IEFy, the EEJ exhibits a significant enhancement reaching the maximum of about 123 nT. This indicates that, during the rapid southward excursion of IMF Bz, the enhanced interplanetary electric field (IEFy) caused a prompt penetration leading to the enhancement in the zonal electric field and EEJ over Brazil. After a rapid increase around 1240 UT, the IEFy exhibits a momentary drop around 1330 UT with the onset of substorm. It can also be seen from Figure 3d that the EEJ also exhibits a small fluctuation (decrease) around 1330 UT coinciding with the momentary fall in IEFy. However, both IEFy and EEJ remained strongly positive during 1200–1400 UT including the substorm episode except for a small fluctuation at ~ 1330 UT. Hence, we mark this enhanced EEJ phase of the storm between 1200–1400 UT as a PPEF-1 phase. Around 1400–1415 UT, both the IEFy and EEJ briefly become negative (Figures 3a and 3d) due to brief northward turning of IMF Bz (Figure 2c). The IEFy subsequently become positive and remained mostly positive (IMF Bz is steadily southward) during 1415–1725 UT and both *AL* and *Wp* indices exhibit several smaller fluctuations. The EEJ (Figure 3d) also exhibits several smaller fluctuations and remains mostly positive, however, smaller than its quiet time reference curve during 1415–1725 UT. Later at ~ 1725 UT, the *Wp* index exhibits a large enhancement, simultaneously with a sudden increase (decrease) in *AE* (*AL*) evidencing the onset of another substorm. The EEJ increases coherently indicating a sudden enhancement in the equatorial zonal electric field due to convective electric field penetration induced by

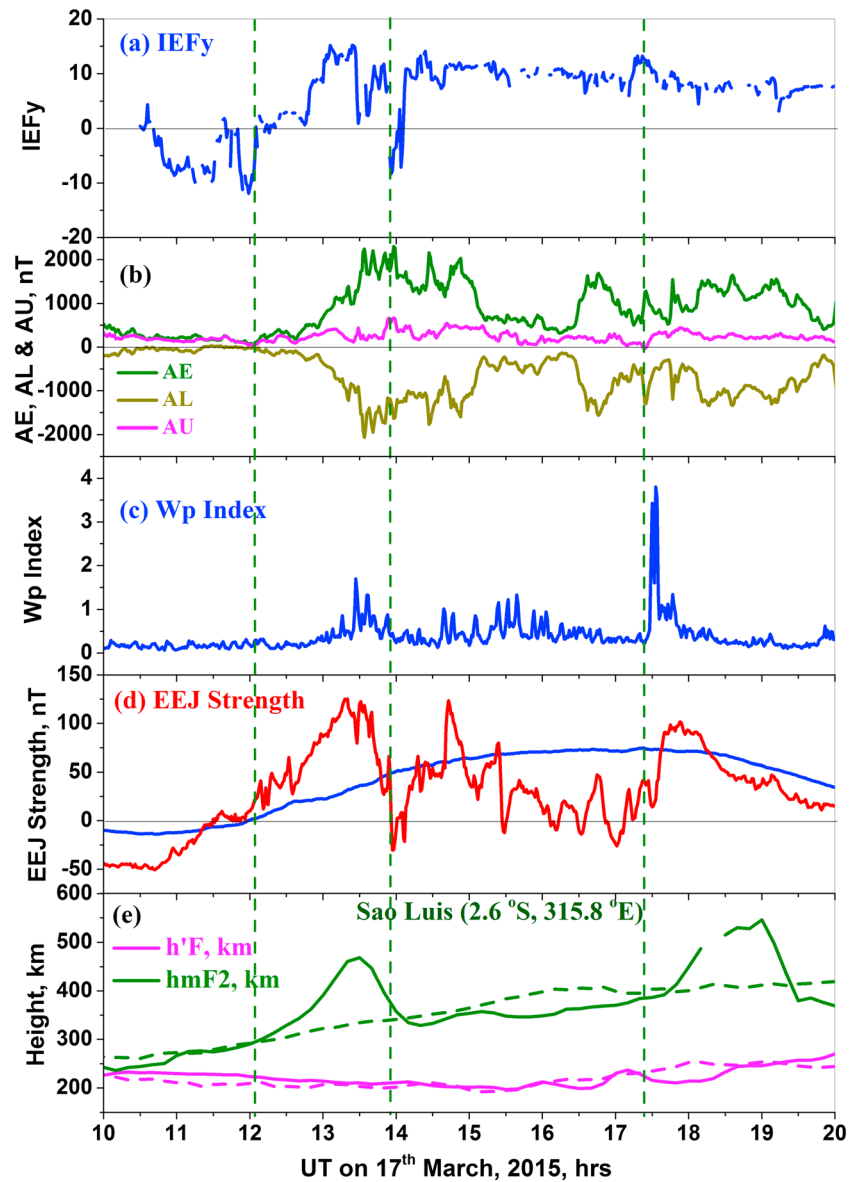


Figure 3. The variations of (a) IEFy, (b) AE, AL, AU, (c) Wp index, (d) EEJ strength, (f) $h'F$, and h_mF_2 over an equatorial station Sao Luis from 1000 to 2000 UT during the main phase of the storm on 17 March 2015.

this substorm at ~1725 UT under the steady southward IMF Bz (eastward IEFy) conditions in the background. We denote this second enhanced EEJ phase of the storm between 1725 and 1900 UT as PPEF-2 phase.

In order to see the resultant modifications in the equatorial ionospheric F layer due to these enhanced zonal electric field conditions, the variations of F layer virtual height ($h'F$) and F layer peak height (h_mF_2) over an equatorial station Sao Luis (SALU) are presented as magenta and green colored curves, respectively, in Figure 3e. The quiet day mean variations of h_mF_2 and $h'F$ from SALU were also presented as dotted lines for comparison. It is observed that the F layer peak height over the equator increased significantly from its quiet time reference value with the enhanced EEJ during the PPEF-1 phase and reached a maximum altitude of 465 km around 1330 UT. Interestingly, $h'F$ variation indicate that the base height of the F layer did not show any uplift during this PPEF-1 phase. Similarly, a large enhancement in h_mF_2 without a significant rise in $h'F$ is also observed during 1725–1900 UT (PPEF-2 phase). Between 1415 and 1725 both the h_mF_2 and $h'F$ more or less remain around their quiet time values with a slight decrease in h_mF_2 . In rest of this paper, we mainly focus our investigation to the equatorial ionospheric response to these enhanced EEJ (zonal electric fields) associated with the two PPEF phases (PPEF-1 and PPEF-2) during the main phase of the St. Patrick's Day storm.

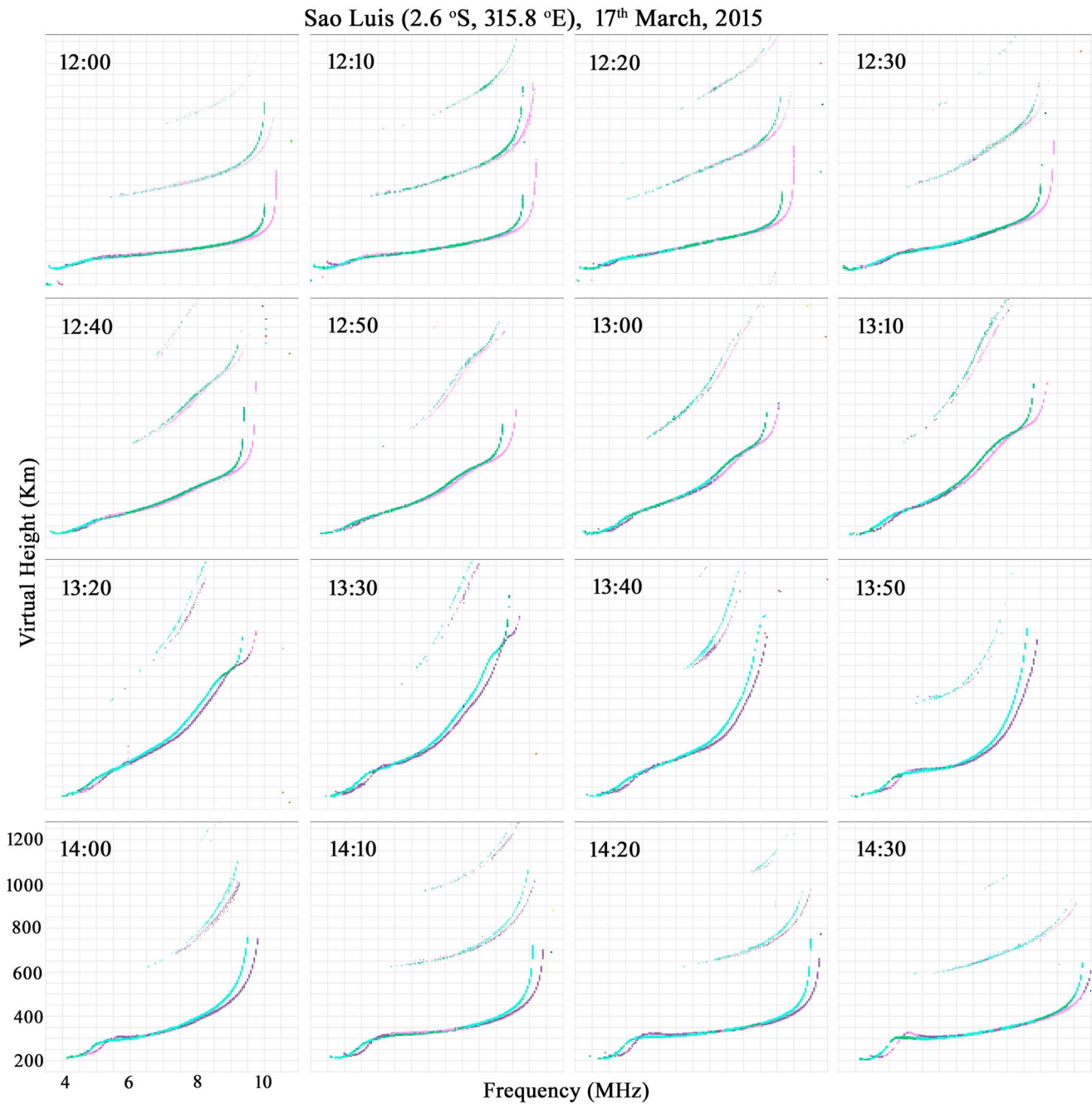


Figure 4. Snapshots of the ionograms over an equatorial station Sao Luis showing the presence of a vertical expansion of F layer along with the occurrence of F_3 layer due to the enhanced zonal electric field during PPEF-1 phase.

The resultant redistribution of ionization and modifications in the EIA structure along the Brazilian longitudinal sector is investigated in detail in the following sections.

3.1. Equatorial F Layer Response and EIA Variations During PPEF-1 Phase

It is interesting to note that the height of the equatorial ionospheric F_2 layer peak ($h_m F_2$) experienced a rapid uplift without any significant rise in the base height ($h'F$) during the PPEF phases (Figure 3e). With a view to further examine the redistribution of plasma at equatorial latitudes in the presence of enhanced zonal electric fields, the snapshots of the ionograms at each 10 min time interval from 1200 to 1430 UT over the equatorial station SALU are presented in Figure 4. The time sequence of ionograms starts at the top left to right

and later to the next row and so on. It is seen from this figure that at 1200 UT, i.e., before the electric field penetration, the F layer is at the low altitudes as usually seen under quiet conditions. Starting from 1210 UT (around the PPEF-1 phase), the F_2 layer peak is drifting upward to higher altitudes in the presence of enhanced zonal electric field while the $h'F$ remains steadily around ~ 200 km. During the uplift of the F_2 layer peak, the maximum density (N_mF_2) is found to be decreased. The diurnal variations of $h'F$ and h_mF_2 presented in Figure 3e have also shown the uplift only in the h_mF_2 without any change in the $h'F$. Further, while the F_2 layer peak is drifting upward, the F_2 layer is redistributed into F_2 and F_3 layers which can be clearly seen in the ionogram at 1240 UT. Further, the observed F_3 layer found to drift upward to higher altitudes between 1240 and 1330 UT and finally disappeared by 1340 UT. Later, the F_2 layer gradually descended to lower altitudes by around 1430 UT. These observations indicate that the F_2 layer peak over the equator experienced a rapid uplift and redistributed into F_2 and F_3 layers due to the enhanced zonal electric fields associated with PPEF-1 phase.

With a view to further investigate the effects of penetration electric fields on the latitudinal distribution of TEC, the diurnal variations of GPS-TEC from equator to the anomaly crest location and beyond along the 315°E longitudinal sector over Brazil during 17 and 18 March, 2015 are presented in Figure 5. These stations lie at the 3 UT time zone, and the shaded region indicates the local nighttime period at these GPS receiver locations. The blue colored curves represent the mean diurnal variations of TEC during five quiet days before the storm. The simultaneous Dst variations are presented in the first row. It is readily seen from this figure that the TEC shows significant deviations from the quiet time behavior at all locations in response to the geomagnetic storm. It is in general noticed that the TEC shows a positive storm effect during the main phase on 17 March 2015 at all latitudes. During the late recovery phase, the daytime TEC over the equator is found to vary nearly around the quiet time levels while a strong negative storm effect is noticed toward the low latitudes. However, the present study is mainly focussed on the TEC response during main phase of the storm. It is observed that, after 1400 UT, the TEC exhibits a rapid increase with a positive storm effect at all locations from equator to the anomaly crest and beyond. This shows that the rapid increase in TEC started nearly after the maximum height rise in the F layer peak over the equator due to the PPEF-1 phase. It is observed that the TEC shows the maximum positive peak around 1630 UT. It can be noticed from the green colored vertical dotted line at 1630 UT that there is a slight time delay from equator toward the low latitudes in reaching the maximum peak during this positive storm effect. After attaining the peak value, the TEC at all the latitudes decreases toward the quiet time levels as rapid as it raised. After the decrease with small depletion, the TEC found to exhibit another positive peak which will be discussed in the later part of the manuscript. The above observations indicate that, during the PPEF-1 phase, after the F peak attaining the maximum altitude due to enhanced zonal electric field, the TEC shows a rapid enhancement with a positive storm effect from equator to the anomaly crest locations and beyond.

In order to understand the spatiotemporal characteristics of TEC and resultant modifications in the EIA structure during the positive storm effect after the PPEF-1, the TEC maps have been made using the GPS observations from 120 receivers all over Brazil. The VTEC values at each GPS location is considered, and the TEC at each 1° latitude and longitude is interpolated using a Matlab routine. Those TEC values are used to make a contour map of TEC over the Brazilian sector. Figure 6 shows the TEC maps over Brazil at each 30 min intervals from 1430 to 1830 UT which corresponds to the period of enhanced TEC peak after the PPEF-1. The geomagnetic equator is shown as black colored curve in each TEC map. It is seen from these maps that, initially, the TEC rapidly builds up around the equatorial latitudes in the Southern Hemisphere. The TEC is found to reach the maximum value around 1630 UT at and near the equator. This is consistent with the TEC peak observed in the diurnal variations presented in Figure 5. The maps at 1630 and 1700 UT show that the TEC is significantly enhanced all over the Brazilian sector. Later, the enhanced plasma is found to move away from the equator which is expected to be associated with the development of the EIA under the fountain effect. Further, it is seen from the maps between 1730 and 1830 UT that the enhanced plasma strongly moved away from the equator toward the low midlatitudes beyond the Brazilian sector. Hence, to study the complete latitudinal structure of EIA during this period along the Brazilian longitudes, the TEC measurements from the world-wide GPS network at Madrigal database are considered. The variations of TEC in the Northern and Southern Hemispheres from -60° to 60° latitudes along the Brazilian longitudes (300° to 315°E) from 1432 to 1832 UT are presented as scatter plots in Figure 7. The red colored dots represent the TEC variations on the storm day of 17 March 2015, while the blue colored dots represent the quiet time TEC variations on 16 March 2015. The region between two vertical blue lines in each panel indicates the geomagnetic equatorial zone. It is seen

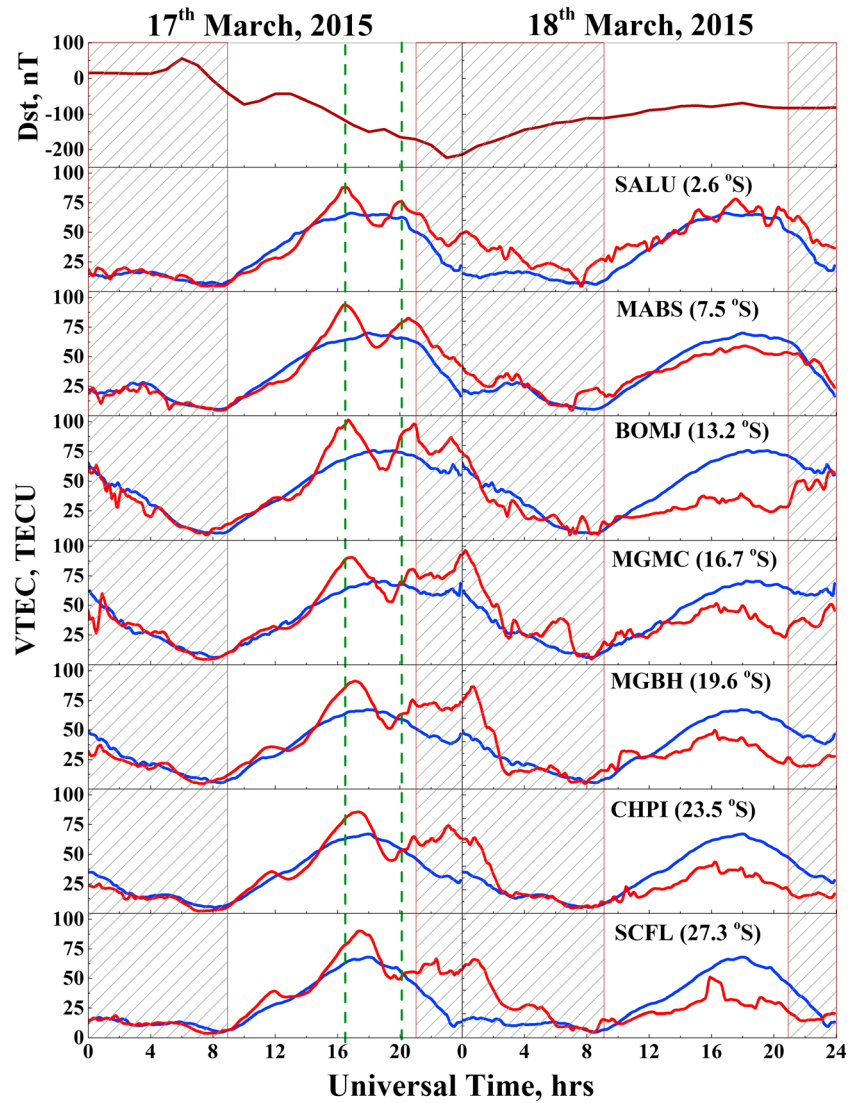


Figure 5. The diurnal variations of GPS-TEC from equator to the anomaly crest locations and beyond along with the *Dst* variations (first row) during 17 and 18 March 2015. The blue colored curves are the quiet time mean variations of TEC.

from this figure that, after 1430 UT, the TEC enhances significantly all over Brazil while the enhancement is found to be more rapid over the equator. The maximum enhancement in TEC with the peak over equator is well pronounced at 1632 UT which is well consistent with the observations made using the TEC maps over the Brazilian sector (Figure 6). After 1630 UT, the enhanced plasma over the equator moved far beyond the equator toward the low midlatitudes under the super fountain effect. It is observed from this figure that the super fountain effect lead to the well-developed EIA around 1732 UT with the southern anomaly crest at nearly 40°S latitudes. It can be observed from this figure that the anomaly crest is located below 20°S latitudes during the previous (quiet) day. Climatological studies over the Brazilian sector have also shown that the anomaly crest usually lies below 20°S latitudes [Cesaroni *et al.*, 2015]. Further, the hemispheric asymmetry in the formation of the EIA is clearly noticed from different panels in this figure as it is seen that the northern anomaly crest is found to be confined below 20°N latitudes.

The above observations indicate that the penetration electric field during the PPEF-1 phase resulted in a significant enhancement in the zonal electric field in the Brazilian sector. In the presence of enhanced zonal electric field, the equatorial ionospheric *F* peak experienced a rapid uplift leading to the super fountain effect. Here it is important to recall that another substorm occurred around 1725 UT initiating PPEF-2 phase which is

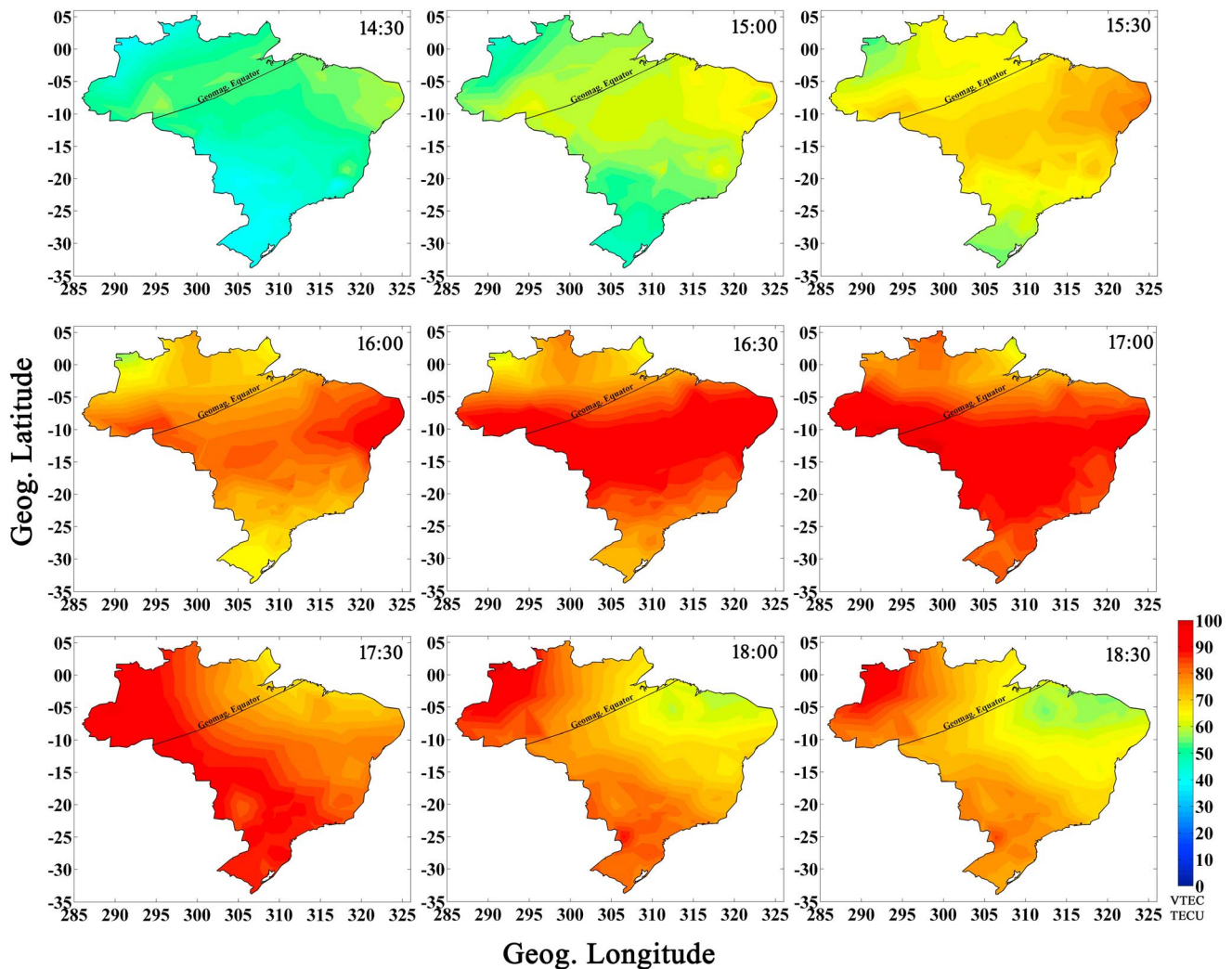


Figure 6. A sequence of TEC maps over Brazil derived using the GPS measurements from 1430 to 1830 UT on 17 March 2015 showing the strong positive ionospheric storm effects all over the Brazil due to the PPEF-1 induced super fountain effect.

just after the super fountain effect due to the PPEF-1. The following section will discuss the influence of PPEF-2 induced zonal electric fields on the equatorial electrodynamic and electron density distribution.

3.2. Equatorial F Layer Response and EIA Variations During PPEF-2 Phase

As it is mentioned earlier, the substorm occurred at 1725 UT induced a penetration of convective electric field causing the secondary enhancement of zonal electric field over the Brazilian longitudes leading to the PPEF-2 phase. The equatorial ionospheric F layer exhibited a similar response during the PPEF-2 phase as it is seen during the PPEF-1 phase. The $h_m F_2$ exhibited a large increase without any significant rise in $h'F$ which was observed from Figure 3e. A series of ionograms at regular intervals from 1730 to 2000 UT over an equatorial station SALU is presented in Figure 8. It is seen from these ionograms that, while the F_2 layer peak is drifting upward, the peak density ($N_m F_2$) reduced and subsequently redistributed in to F_2 and F_3 layers which can be clearly seen after 1800 UT. The F_3 layer found to drift further upward to higher altitudes during 1810–1910 UT and finally disappeared by 1920 UT. All these modifications in the equatorial F layer such as rapid uplift of $h_m F_2$ (without any rise in $h'F$), reduction in $N_m F_2$ and redistribution into F_2 and F_3 layers are consistently observed during the both PPEF phases.

The TEC variations presented earlier in Figure 5 shows that, after the first positive peak due to the PPEF-1, the TEC decreased and showed a small depletion around 1830 to 1900 UT. Later, the TEC again increased rapidly

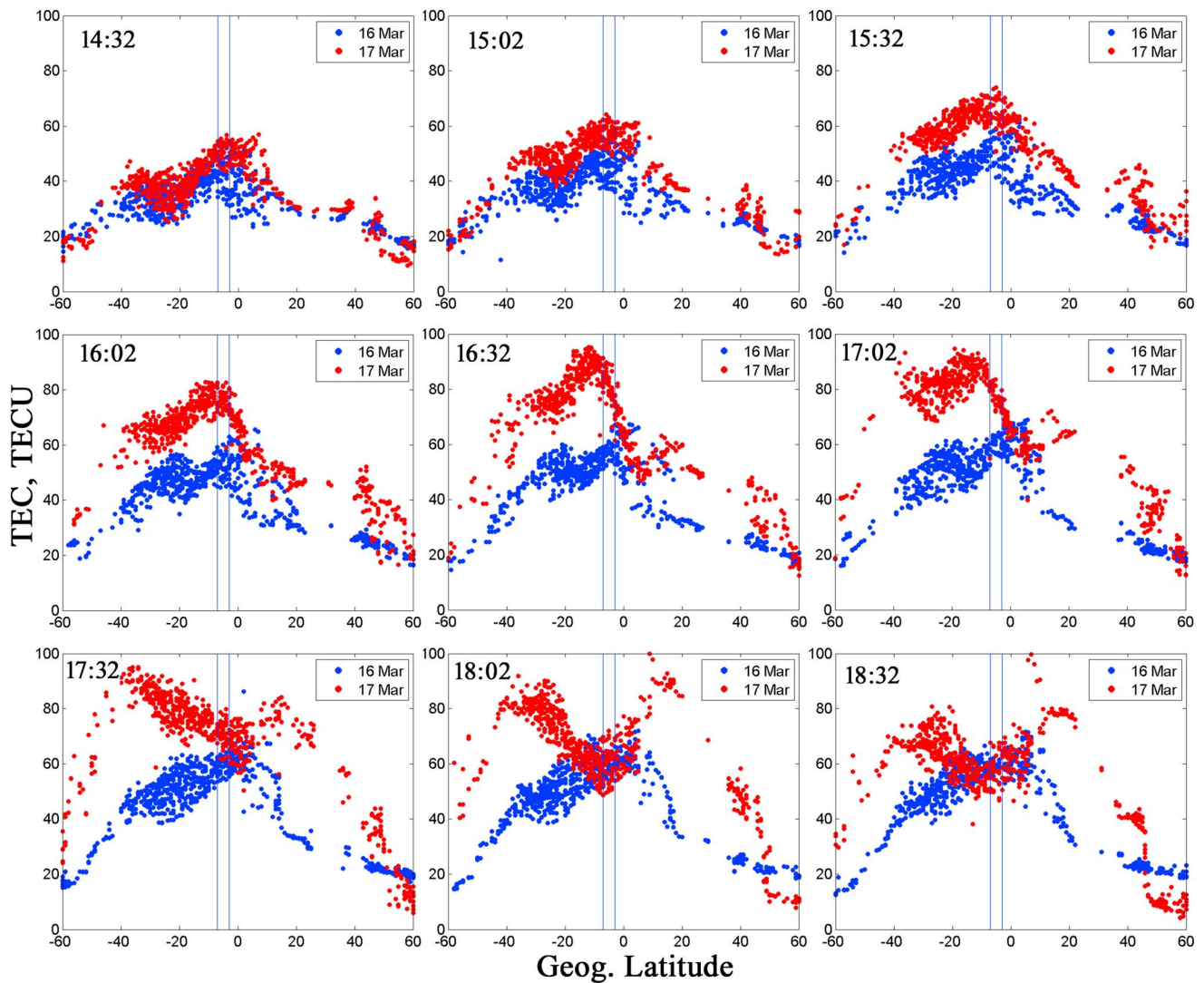


Figure 7. Latitudinal variations of storm time TEC at each 30 min interval from 1432 to 1832 UT on 17 March 2015 (red colored scatters) from -60° to 60° latitudes along the Brazilian longitude sector showing the development of a super fountain effect in the Southern Hemisphere after first substorm expansion. The simultaneous quiet time TEC variations on 16 March 2015 are presented as blue colored scatters.

showing a secondary peak near 2000 UT at and around the equatorial latitudes. Away from the equator, the TEC increases gradually toward the late night hours showing a strong positive storm effect. The TEC diurnal variations indicate that the second positive enhancement is clearly following the *F* layer peak rise during the PPEF-2 phase. Hence, to study the spatiotemporal response of TEC to the PPEF-2, the TEC maps all over Brazil at regular intervals of 30 min from 1830 to 2230 UT are presented in Figure 9. It is clearly noticed from this figure that, after 1830 UT, the TEC started increasing over the equatorial and southern low latitudes. Near the equator the maximum TEC is seen around 2000 UT. Later, the increased plasma over the equator further enhanced and moved away toward the low latitudes leading to the formation of EIA for the second time. It is observed that the well-developed EIA is seen around 2100 UT with the anomaly crest located at $\sim 20^{\circ}$ S latitudes. To further see the latitudinal response in the Northern and Southern Hemispheres during this period, the latitudinal variations of TEC from -60° to 60° latitudes along the Brazilian longitudinal sector at each 30 min interval from 18:32 to 22:32 are presented in Figure 10. The red colored scatters show the TEC variations on 17 March 2015, while the blue colored scatters represent those on 16 March 2015. It is seen from this figure that the TEC at 1900 UT is mostly around the quiet time level all over Brazil which is consistent with the TEC depletion seen in the diurnal variations presented in Figure 5. After 1900 UT, the TEC started building up near the equator, and the

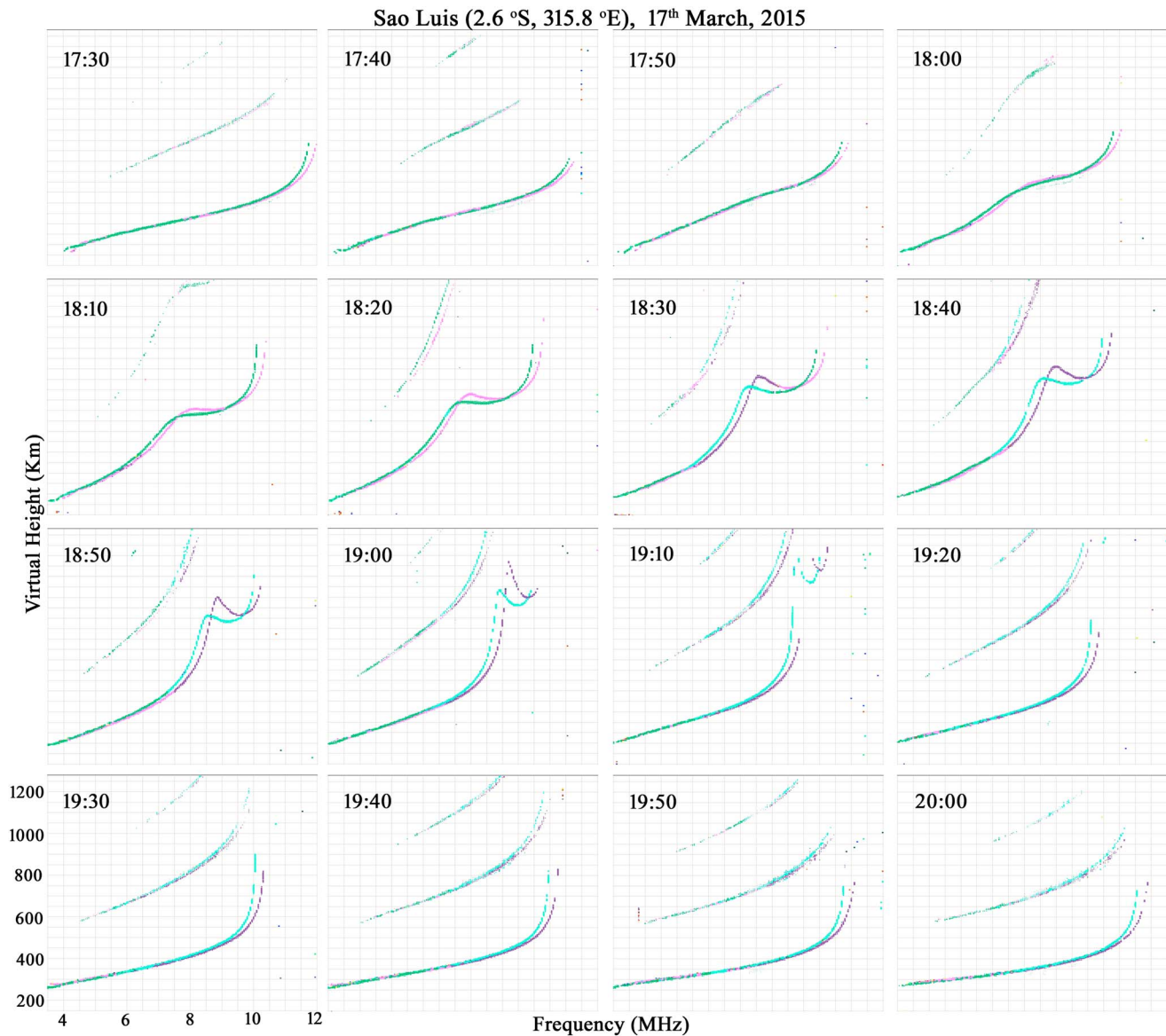


Figure 8. Snapshots of the ionograms over an equatorial station Sao Luis at regular time intervals from 1730 to 2010 UT showing the presence of a vertical expansion of *F* layer along with the occurrence of *F*₃ layer due to the in the presence of enhanced zonal electric field during PPEF-2 phase.

enhanced plasma moved away toward the southern low latitudes. The well-developed EIA in the Southern Hemisphere is found around 2100 UT with the anomaly crest located at ~20°S latitudes. Also, the EIA asymmetry is clearly noticed between Northern and Southern Hemispheres. In the Northern Hemisphere, the anomaly strength is found to be much weaker compared to that in the Southern Hemisphere and the northern crest is confined around 10°N latitude.

The above TEC observations indicate that, following the *F* layer peak uplift during the PPEF-2 phase, the TEC enhanced over the equator leading to the formation of a strong EIA. These features of TEC after the PPEF-2 are similar to those observed after the PPEF-1. However, during the PPEF-1 super fountain effect is noticed with the southern anomaly crest around 40°S latitudes while after the PPEF-2, the anomaly crest is found to be confined around 20°S latitudes. The spatiotemporal disturbances of TEC in the Brazilian sector due to both PPEF phases can be seen with 1 min time resolution in Movie S1 presented in the supporting information. Further, the storm time modifications of EIA due to super fountain effect and the interhemispheric asymmetry along the Brazilian longitudinal zone during the both PPEF phases can be seen with 5 min time resolution in Movie S2 which is presented in the supporting information.

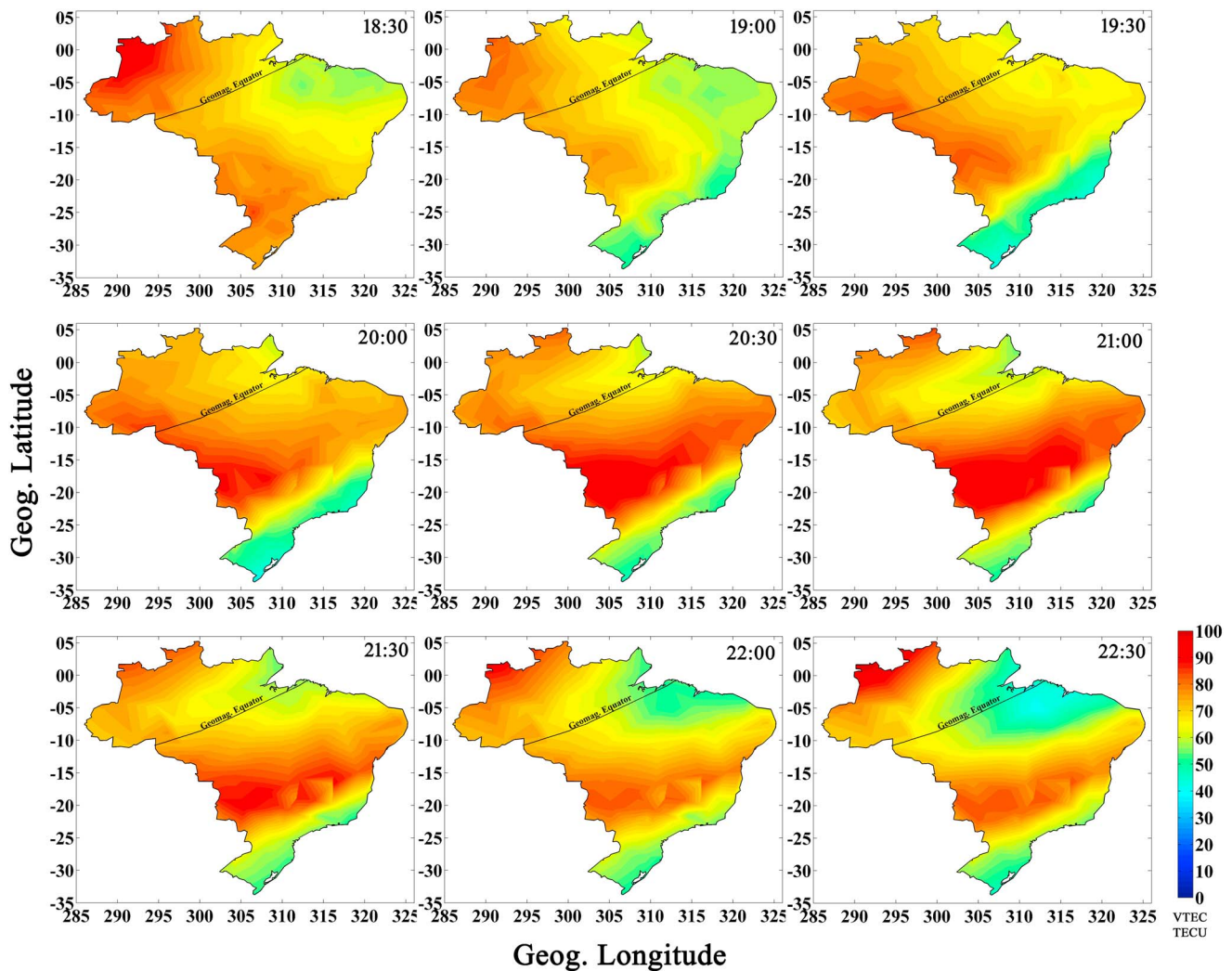


Figure 9. A sequence of TEC maps over Brazil derived using the GPS measurements from 1830 to 2230 UT on 17 March 2015 showing a strong anomaly crest with positive ionospheric storm effect due to the PPEF-2 phase.

4. Discussion

The strongest geomagnetic storm so far during the 24th solar cycle occurred on the St. Patrick's Day of 17 March 2015 with the minimum Dst of -223 nT. During the main phase of the storm, the Brazilian region lies in the morning-afternoon sector facilitating to understand the storm time response of zonal electric field and its influence on the daytime equatorial electrodynamics. It is observed that the IMF B_z turned southward around 1200 UT on 17 March 2015 followed by a rapid negative excursion at 1240 UT. As a result, the IEFy experienced a strong enhancement causing a prompt penetration of electric field leading to an enhancement in the zonal electric field over the Brazilian sector. This enhanced zonal electric field phase lasted up to ~ 1400 UT which is termed as PPEF-1 phase. Later, the onset of a substorm around 1725 UT caused another PPEF and resulted in rapid enhancement in the zonal electric field over Brazil which is termed as PPEF-2 phase. The penetration of substorm-induced electric fields from high latitudes to low latitudes is reported by several studies during other storm events [Gonzales *et al.*, 1979; Kikuchi *et al.*, 2003; Sastri *et al.*, 2003b; Huang, 2012]. It has been reported earlier that the zonal electric field disturbance is eastward during daytime at the low latitudes with the positive geomagnetic field disturbance under southward IMF B_z during the storm time substorm [Huang *et al.*, 2004 and Huang, 2009, 2012]. Huang [2009, 2012] reported that the increased convection at substorm onset causes an enhanced magnetosphere electric field which penetrates into the dayside low-latitude ionosphere resulting in an enhanced zonal electric field.

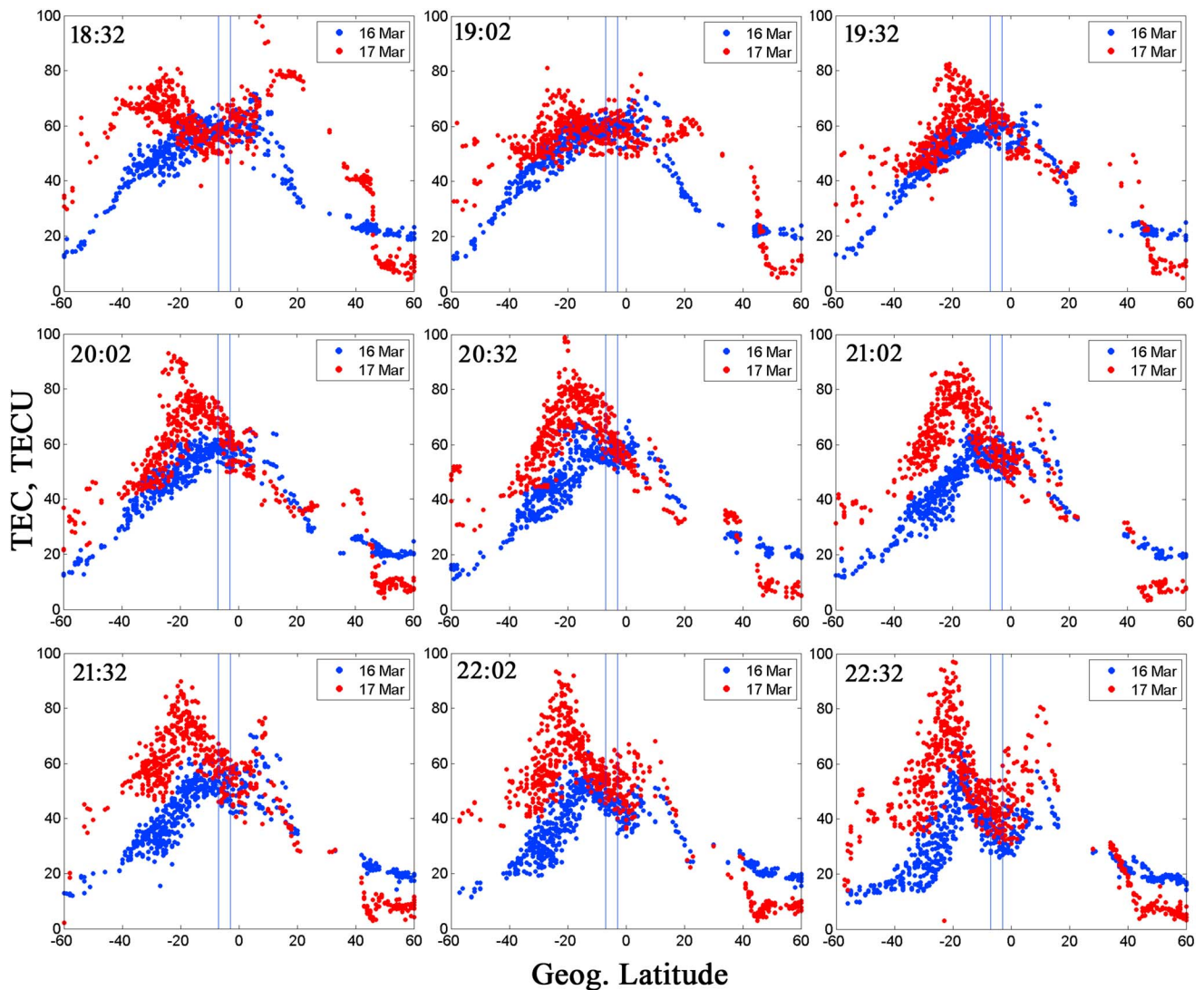


Figure 10. Latitudinal variations of storm time TEC at each 30 min interval from 1832 to 2232 UT on 17 March 2015 (red colored scatters) from -60° to 60° latitudes along the Brazilian longitude sector showing the formation of EIA after the second substorm. The simultaneous quiet time TEC variations on 16 March 2015 are presented as blue colored scatters.

A detailed insight into the ionograms during the two PPEF phases (Figures 4 and 8) indicated that, in the presence enhanced zonal electric field, the F layer peak experienced a strong uplift without any change in the base height along with a decrease in the F layer peak density. Further, it is also noticed that the enhanced electric fields due to PPEF caused vertical redistribution of equatorial plasma via $E \times B$ drift and resulted as the additional stratification of F_3 layer, without any rise in the base height ($h'F$) of the layer. The additional stratification of F_3 layer due to PPEF in the dayside equatorial region has been observed earlier by *Balan et al.* [2008] and *Tulasi Ram et al.* [2012]. The F_3 layer occurrence characteristics during storm time and their comparison with those of quiet time are reported by *Batista et al.* [2017]. The enhanced electric fields transport the equatorial plasma vertically upward; however, Brazilian sector being in dayside, the ion production viz photoionization continuously occurs at F region base around 200 km. Hence, the uplifted plasma around F region base is being quickly refilled by the newly produced plasma by photoionization at those altitudes during daytime [*Balan et al.*, 2008].

During the PPEF-1 phase, in the presence of enhanced zonal electric field, the F layer peak has shown a strong uplift between 1200 and 1400 UT without any change in the base height. The diurnal variations of TEC from equator to the anomaly crest locations in the Brazilian sector (Figure 5) have shown a rapid

enhancement around 1400 UT which is following the F layer vertical expansion due to the PPEF-1 phase. This can be understood as the vertically expanded F layer carried major plasma to the higher altitudes where the recombination rates are lower and the life time of the uplifted plasma becomes longer [Bank and Kockarts, 1973; Hargreaves, 1979]. Simultaneously, more plasma is expected to be produced at the lower altitudes due to the photo ionization process. Therefore, after the F layer expansion, the total amount of ionization keeps increasing and resulted in the TEC enhancement which is seen as a positive ionospheric storm effect in the diurnal variations of TEC. At and around the equator the TEC reaches its maximum positive peak at 1630 UT. The GPS TEC maps in the Brazilian sector (Figure 6) indicated that the uplifted plasma near the equatorial region moved away toward the low latitudes under the fountain effect. It is also noticed that, under the fountain effect, the plasma moved far beyond the Brazilian latitudes as seen from the Brazilian maps between 1700 to 1800 UT in Figure 6. Further, the TEC measurements (from Madrigal base) in the Northern and Southern Hemispheres from -60° to 60° latitudes along the Brazilian longitudinal zone (Figure 7) revealed that the PPEF-1 phase resulted in the super fountain effect in the Brazilian longitudes. Hence, the enhanced plasma moved toward the low midlatitudes under the super fountain effect forming the well-developed EIA at ~ 1730 UT with the anomaly crest located around -40° latitudes.

In the process of super fountain effect due to the PPEF-1 phase, the TEC reached its maximum at 1630 UT around the equator, and later it moved toward the low latitudes. Hence, the maximum TEC during the first positive storm effect is noticed at delayed hours at the low latitudes compared to that at the equator as seen in Figure 5. Also, since the enhanced plasma moved toward the low midlatitudes forming the EIA crest beyond the Brazilian sector at $\sim 40^\circ$ latitudes, the TEC reduced at the Brazilian equatorial and low latitudes which is seen as a depletion in the diurnal variations of TEC (Figure 5). After the well-developed EIA at 1730 UT, the super fountain effect started subsiding which is clearly seen from the Brazilian maps and TEC latitudinal variations in Figures 6 and 7 as well as in Movies S1 and S2. It is important to recall here that the PPEF-2 phase started nearly at the same time around 1725 UT resulting in a rapid enhancement in the zonal electric field for a second time. Hence, while the super fountain effect due to PPEF-1 is subsiding, the PPEF-2 phase took place and caused an enhancement in the zonal electric field.

During the PPEF-2 phase also, the equatorial F layer experienced an upward expansion with a rapid uplift in the F peak keeping the F layer base at the same altitudes (Figure 8) along with the occurrence of F_3 layer which is consistent with the equatorial F layer behavior during the PPEF-1 phase. The F peak reached maximum altitude around 1910 UT, after which it descended down and the F_3 layer disappeared. Similar to that observed during the PPEF-1, during the vertical expansion of the F layer, more plasma is accumulated at higher altitudes (lower recombination rate region). This enhanced the plasma at and around the equator and resulted in a secondary peak in the TEC diurnal variations leading to a positive storm effect as seen in Figure 5. This indicates that the daytime TEC exhibits two positive storm effects due to the two PPEF phases. These observations of two positive peaks are in consistent with those reported by Nava *et al.* [2016] using the regional electron content (REC) measurements. During the second positive storm effect, the enhanced plasma near the equator shows maximum around 2000 UT. This uplifted plasma near the equator further enhanced and drifted toward the low latitudes under the fountain effect which is clearly seen from the Brazilian TEC maps (Figure 9) and latitudinal variations of TEC (Figure 10) after 2000 UT. The well-developed anomaly is seen around 2130 UT, and the EIA crest is located around 20° southern latitudes. As it is evidenced from the TEC maps, the electron density initially enhanced near the equator reaching the peak around 2000 UT and later propagated to the lower latitudes forming the EIA crest and resulting in a strong positive storm effect toward the late evening hours at the anomaly crest locations. The positive storm effect during the main phase of this storm in the Brazilian sector was mentioned by Fagundes *et al.* [2016]. However, they have not explored the presence of penetration electric fields to explain the storm time ionospheric response. The present study clearly demonstrates the occurrence of two PPEF phases; their influence on the equatorial zonal electric field and F layer (using simultaneous ionosonde and EEJ observations) along with a detailed discussion on the resultant modifications and the temporal evolution of EIA in the Northern and Southern Hemispheres due to the two PPEF phases.

Comparing the hemispheric asymmetry in the storm time response of EIA, during the PPEF-1 induced super fountain, the anomaly crest in the Southern Hemisphere is stronger (~ 90 total electron content units (TECU), $1 \text{ TECU} = 10^{16} \text{ el m}^{-2}$) and farther (40° S) than the EIA crest in the Northern Hemisphere

which is confined below 20°N latitude as seen in Figure 7. During the PPEF-2 effect also (Figure 10), the southern EIA crest is stronger (~90 TECU) and located around 20°S latitudes compared to the northern anomaly crest (~70 TECU) which is confined around 10°N latitudes. The hemispheric asymmetry of positive/negative ionospheric TEC storms that usually occur during the solstices is generally attributed to the asymmetry in the storm time disturbed neutral winds during solstices [Buonsato, 1999] and associated composition changes. However, the present storm occurred close to spring equinox day. *Tulasi Ram et al.* [2015] have shown the presence of strong westward and equatorward wind surge from Shigaraki (Japan) and Darwin (Australia), the conjugate midlatitude locations in Northern and Southern Hemispheres, respectively, in the nightside which indicates the ionospheric disturbance dynamo effects. This storm time disturbance neutral winds maximized to 100–250 m/s in westward and 200–300 m/s in equatorward [Tulasi Ram et al., 2015, Figure 5]. *Zhang et al.* [2017] have shown strong equatorward neutral wind surge (> 200 m/s) from the Millstone Hill radar in the dayside (American sector) consistently with nightside observations of *Tulasi Ram et al.* [2015]. *Huang et al.* [2016] have also reported that there was a disturbance dynamo process initiated 3–4.7 h after the onset of the storm main phase and lasted for 31 h. Hence, it is expected that strong equatorward and westward neutral wind disturbance is also operating in the dayside Brazilian sector. The equatorward neutral wind transports the plasma along the inclined magnetic field lines to the higher altitudes where the loss due to recombination is less. Further, the westward neutral wind is also effective in the upward/downward transport of plasma at the regions of higher declination angles of field lines [Titheridge, 1995]. The westward and equatorward wind surge is more effective in the Southern Hemisphere of Brazilian sector because of large westward declination and negative (upward) inclination angles of field lines. This would explain the large enhancements in TEC in the southern low midlatitudes compared to their northern conjugate latitudes observed in Figures 7 and 10.

Further, comparing the ionospheric response to the two PPEF phases, the influence is stronger during the PPEF-1 phase than that during the PPEF-2 phase. During the PPEF-1, the TEC is strongly enhanced all over the Brazilian latitudes with a super fountain effect forming the crest around 40°S latitude. During the PPEF-2, the anomaly is confined to 20°S latitudes and the EIA strength is comparably weaker than the first event. This has some evidence from the EEJ variations (Figure 3d) where the zonal electric field enhancement during the PPEF-1 phase is stronger (~123 nT) compared to that during the PPEF-2 (~100 nT). Also, during the PPEF-1 phase, the ionization is building up in the Brazilian sector as well as the integrated EEJ strength is stronger which might have given an added strength for the formation of a super fountain effect.

5. Summary

The dayside equatorial ionospheric response over Brazilian sector during the main phase of the St. Patrick's Day storm on 17 March 2015 has been investigated using simultaneous observations from ground-based ionosondes, magnetometers, and a large network of 120 GPS receivers from IBGE network complemented by GPS observations in the South and North American sectors from Madrigal database. The salient findings from this study are summarized here under.

1. The dayside equatorial zonal electric field disturbances are dominated by two strong PPEF phases, one at ~1200 UT with the southward turning of IMF Bz and another at ~1725 UT with the onset of substorm.
2. During both the PPEF phases, the enhanced zonal electric field resulted in a vertical expansion of the equatorial F layer peak without any significant change in the base height. While the F peak is drifting vertically upward, it is found that the F_2 layer is redistributed into F_2 and F_3 layers.
3. During the F layer upward expansion, more plasma is moved to the higher altitudes where the recombination rates are lower. The simultaneous production of ionization at the lower altitudes lead to an enhancement in TEC resulting in a strong positive ionospheric storm effect.
4. The enhanced zonal electric field due to PPEF-1 resulted in equatorial super fountain that caused the poleward departure of EIA crest to ~40°S latitudes.
5. The equatorial F layer experienced a similar kind of response during the PPEF-2 phase leading to the fountain effect for the second time. As a result, the well-developed anomaly is seen around 2100 UT with the anomaly crest located at ~20°S latitudes.
6. During both the PPEF phases, significant asymmetry in the EIA storm time response is clearly noticed where the southern EIA crest is stronger and farther to the equator.

7. In the presence of storm time disturbance dynamo, westward and equatorward wind surge is more effective in the Southern Hemisphere of Brazilian sector because of large westward declination and negative (upward) inclination angles of field lines which could have caused the strong hemispheric asymmetry in the storm time TEC response.
8. Between the two PPEF phases, the PPEF-1 influence is more intense leading to the super fountain effect with the southern anomaly crest around low midlatitudes at 40°S. This could be due to the strong enhancement in the zonal electric field during the PPEF-1. In addition, the building up of ionization during the PPEF-1 phase might strengthened the positive storm effect leading to the super fountain effect.

Acknowledgments

One of the authors, K.V., wishes to express his sincere thanks to the Fundação de Amparo a Pesquisa do Estado de São Paulo (FAPESP), São Paulo, Brazil, for providing financial support through the process 2012/08445-9 and 2013/17380-0. The authors wish to express their sincere thanks to IBGE (http://www.ibge.gov.br/home/geociencias/geodesia/rbmc/rbmc_est.php) for providing GPS-TEC data over Brazil; the GIRO and UML DID Base (<http://ulcar.uml.edu/DIDBase/>; <http://spase.info/SMWG/Observatory/GIRO>) for providing ionosonde data over São Luis; C.M. Denardini, INPE, Brazil, for providing magnetometer data over Eusebio; E. Yizengaw, E. Zesta, M. B. Moldwin, and the rest of the AMBER and SAMBA team for the magnetometer data over Belem being operated by Boston College and funded by NASA and AFOSR; The Space Physics Data Facility (SPDF), NASA, USA (http://omniweb.gsfc.nasa.gov/ow_min.html) for the solar wind parameters, IMF Bz, SYM-H, AU, and AL indices; the World Data Centre (WDC) for Geomagnetism, Kyoto (<http://wdc.kugi.kyoto-u.ac.jp/dstdir/index.html>) for the Dst values and quiet day information; and Kyoto University, Japan, for the online Wp index data (<http://s-cubed.info/index.html>). The madrigal TEC data is downloaded from the website (<http://madrigal.haystack.mit.edu/cgi-bin/madrigal/madInvent.cgi>). GPS TEC data products and access through the Madrigal distributed data system are provided to the community by the Massachusetts Institute of Technology under support from U.S. National Science Foundation grant AGS-1242204.

References

- Astafyeva, E., I. Zakharenkova, and M. Förster (2015), Ionospheric response to the 2015 St. Patrick's Day storm: A global multi-instrumental overview, *J. Geophys. Res. Space Physics*, *120*, 9023–9037, doi:10.1002/2015JA021629.
- Bank, P. M., and G. Cockart (1973) *Aeronomical Reactions in Aeronomy Part A*, pp. 240–289, Academic Press, New York and London.
- Balan, N., S. V. Thampi, K. Lynn, Y. Otsuka, H. Alleyne, S. Watanabe, M. A. Abdu, and B. G. Fejer (2008), F_3 layer during penetration electric field, *J. Geophys. Res.*, *113*, A00A07, doi:10.1029/2008JA013206.
- Balan, N., J. Y. Liu, Y. Otsuka, S. Tulasi Ram, and H. Lühr (2012), Ionospheric and thermospheric storms at equatorial latitudes observed by CHAMP, ROCSAT, and DMSF, *J. Geophys. Res.*, *117*, A01313, doi:10.1029/2011JA016903.
- Batista, I. S., C. M. N. Candido, J. R. Souza, M. A. Abdu, R. C. de Araujo, L. C. A. Resende, and A. M. Santos (2017), F_3 layer development during quiet and disturbed periods as observed at conjugate locations in Brazil: The role of the meridional wind, *J. Geophys. Res. Space Physics*, *122*, 2361–2373, doi:10.1002/2016JA023724.
- Blanc, M., and A. Richmond (1980), The ionospheric disturbance dynamo, *J. Geophys. Res.*, *85*, 1669–1686, doi:10.1029/JA085iA04p01669.
- Buonsato, M. J. (1999), Ionospheric storms—A review, *Space Sci. Rev.*, *88*, 563–601, doi:10.1023/A:1005107532631.
- Cesaroni, C., L. Spogli, L. Alfonsi, G. De Franceschi, L. Ciralo, J. F. G. Monico, C. Scotto, V. Romano, M. Aquino, and B. Bougard (2015), L-band scintillations and calibrated total electron content gradients over Brazil during the last solar maximum, *J. Space Weather Space Clim.*, *5*, A36, doi:10.1051/swsc/2015038.
- Crowley, G., A. Reynolds, J. P. Thayer, J. Lei, L. J. Paxton, A. B. Christensen, Y. Zhang, R. R. Meier, and D. J. Strickland (2008), Periodic modulations in thermospheric composition by solar wind high speed streams, *Geophys. Res. Lett.*, *35*, L21106, doi:10.1029/2008GL035745.
- Danilov, A. D. (2013), Ionospheric F-region response to geomagnetic disturbances, *Adv. Space Res.*, *52*(3), 343–366, doi:10.1016/j.asr.2013.04.019.
- Denardini, C. M., L. C. A. Resende, J. Moro, M. Rockenbach, P. R. Fagundes, M. A. Gende, S. S. Chen, N. J. Schuch, and A. Petry (2013), The South American K index: Initial steps from the embrace magnetometer network, *Proc. of the 13th Int. Congress of the Brazilian Geophys. Soc. & EXPOGEF*, pp. 1901–1905, Rio de Janeiro, Brazil, 26–29 Aug., doi:10.1190/sbgf2013-391.
- Fagundes, P. R., F. A. Cardoso, B. G. Fejer, K. Venkatesh, B. A. G. Ribeiro, and V. G. Pillat (2016), Positive and negative GPS-TEC ionospheric storm effects during the extreme space weather event of March 2015 over the Brazilian sector, *J. Geophys. Res. Space Physics*, *121*, 5613–5625, doi:10.1002/2015JA022214.
- Fejer, B. G. (2002), Low latitude storm time ionospheric electrodynamics, *J. Atmos. Sol. Terr. Phys.*, *64*, 1401, doi:10.1016/S1364-6826(02)00103-7.
- Fejer, B. G., M. F. Larsen, and D. T. Farley (1983), Equatorial disturbance dynamo electric fields, *Geophys. Res. Lett.*, *10*, 537–540, doi:10.1029/GL010i007p00537.
- Field, P. R., and H. Rishbeth (1997), The response of the ionospheric F_2 layer to geomagnetic activity: An analysis of worldwide data, *J. Atmos. Sol. Terr. Phys.*, *59*(2), 163–180, doi:10.1016/S1364-6826(96)00085-5.
- Förster, M., and N. Jakowski (2000), Geomagnetic storm effects on the topside ionosphere and plasmasphere: A compact tutorial and new results, *Surv. Geophys.*, *21*, 47–87, doi:10.1023/A:1006775125220.
- Fuller-Rowell, T. J., M. V. Codrescu, R. J. Moffett, and S. Quegan (1994), Response of the thermosphere and ionosphere to geomagnetic storms, *J. Geophys. Res.*, *99*, 3893–3914, doi:10.1029/93JA02015.
- Fuller-Rowell, T. J., M. V. Codrescu, H. Rishbeth, R. J. Moffett, and S. Quegan (1996), On the seasonal response of the thermosphere and ionosphere to geomagnetic storms, *J. Geophys. Res.*, *101*, 2343–2353, doi:10.1029/95JA01614.
- Gonzales, C. A., M. C. Kelley, B. G. Fejer, J. F. Vickrey, and R. F. Woodman (1979), Equatorial electric fields during magnetically disturbed conditions: 2. Implications of simultaneous auroral and equatorial measurements, *J. Geophys. Res.*, *84*, 5803–5812, doi:10.1029/JA084iA10p05803.
- Hargreaves, J. K. (1979) *The Upper Atmosphere and Solar-Terrestrial Relations—An Introduction to the Aerospace Environment*, pp. 52–87, Van Nostrand Reinhold Co., New York.
- Huang, C.-S., J. C. Foster, L. P. Goncharenko, G. D. Reeves, J. L. Chau, K. Yumoto, and K. Kitamura (2004), Variations of low-latitude geomagnetic fields and Dst index caused by magnetospheric substorms, *J. Geophys. Res.*, *109*, A05219, doi:10.1029/2003JA010334.
- Huang, C.-S., J. C. Foster, L. P. Goncharenko, P. J. Erickson, W. Rideout, and A. J. Coster (2005), A strong positive phase of ionospheric storms observed by the Millstone Hill incoherent scatter radar and global GPS network, *J. Geophys. Res.*, *110*, A06303, doi:10.1029/2004JA010865.
- Huang, C.-S. (2009), Eastward electric field enhancement and geomagnetic positive bay in the dayside low-latitude ionosphere caused by magnetospheric substorms during sawtooth events, *Geophys. Res. Lett.*, *36*, L18102, doi:10.1029/2009GL040287.
- Huang, C.-S. (2012), Statistical analysis of dayside equatorial ionospheric electric fields and electrojet currents produced by magnetospheric substorms during sawtooth events, *J. Geophys. Res.*, *117*, A02316, doi:10.1029/2011JA017398.
- Huang, C.-S., G. R. Wilson, M. R. Hairston, W. W. Zhang, and J. Liu (2016), Equatorial ionospheric plasma drifts and O+ concentration enhancements associated with disturbance dynamo during the 2015 St. Patrick's Day magnetic storm, *J. Geophys. Res. Space Physics*, *121*, 7961–7973, doi:10.1002/2016JA023072.
- Kelley, M. C., B. G. Fejer, and C. A. Gonzales (1979), An explanation for anomalous equatorial ionospheric electric fields associated with a northward turning of the interplanetary magnetic field, *Geophys. Res. Lett.*, *6*, 301–304, doi:10.1029/GL006i004p00301.
- Kelley, M. C., J. J. Makela, J. L. Chau, and M. J. Nicolls (2003), Penetration of the solar wind electric field into the magnetosphere/ionosphere system, *Geophys. Res. Lett.*, *30*(4), 1158, doi:10.1029/2002GL016321.

- Kikuchi, T., H. Lühr, T. Kitamura, O. Saka, and K. Schlegel (1996), Direct penetration of the polar electric field to the equator during a DP2 event as detected by the auroral and equatorial magnetometer chains and the EISCAT radar, *J. Geophys. Res.*, *101*, 17,161–17,173, doi:10.1029/96JA01299.
- Kikuchi, T., H. Lühr, K. Schlegel, H. Tachihara, M. Shinohara, and T.-I. Kitamura (2000), Penetration of auroral electric fields to the equator during a substorm, *J. Geophys. Res.*, *105*, 23,251–23,261, doi:10.1029/2000JA900016.
- Kikuchi, T., K. K. Hashimoto, T.-I. Kitamura, H. Tachihara, and B. Fejer (2003), Equatorial counter-electrojets during substorms, *J. Geophys. Res.*, *108*(A11), 1406, doi:10.1029/2003JA009915.
- Kuai, J., L. Liu, J. Liu, S. Sripathi, B. Zhao, Y. Chen, H. Le, and L. Hu (2016), Effects of disturbed electric fields in the low latitude and equatorial ionosphere during the 2015 St. Patrick's Day storm, *J. Geophys. Res. Space Physics*, *121*, 9111–9126, doi:10.1002/2016JA022832.
- Mendillo, M. (2006), Storms in the ionosphere: Patterns and processes for total electron content, *Rev. Geophys.*, *44*, RG4001, doi:10.1029/2005RG000193.
- Nava, B., J. Rodríguez-Zuluaga, K. Alazo-Cuartas, A. Kashcheyev, Y. Migoya-Orué, S. M. Radicella, C. Amory-Mazaudier, and R. Fleury (2016), Middle- and low-latitude ionosphere response to 2015 St. Patrick's Day geomagnetic storm, *J. Geophys. Res. Space Physics*, *121*, 3421–3438, doi:10.1002/2015JA022299.
- Nishida, A. (1968), Coherence of geomagnetic DP2 fluctuations with interplanetary magnetic variations, *J. Geophys. Res.*, *73*, 5549–5559, doi:10.1029/JA073i017p05549.
- Nosé, M., et al. (2009), New substorm index derived from high-resolution geomagnetic field data at low latitude and its comparison with AE and ASY indices, in *Proceedings of XIIIth IAGA Workshop on Geomagnetic Observatory Instruments, Data Acquisition, and Processing*, U.S. Geol. Surv. Open File Rep., 2009–1226, edited by J. J. Love, pp. 202–207. [Available at <https://pubs.usgs.gov/of/2009/1226/pdf/OF09-1226.pdf>.]
- Nosé, M., et al. (2012), Wp index: A new substorm index derived from high-resolution geomagnetic field data at low latitude, *Space Weather*, *10*, S08002, doi:10.1029/2012SW000785.
- Prölss, G. W. (1995), Ionospheric F region storms, in *Handbook of Atmospheric Electrodynamics*, Vol. 2, edited by H. Volland, pp. 195–248, CRC Press, Boca Raton, London.
- Rastogi, R. G., and V. L. Patel (1975), Effect of interplanetary magnetic field on ionosphere over the magnetic equator, *Proc. Indian Acad. Sci.*, *82A*, 121–141.
- Reinisch, B. W., and I. A. Galkin (2011), Global Ionospheric Radio Observatory (GIRO), *Earth Planets Space*, *63*(4), 377–381, doi:10.5047/eps.2011.03.001.
- Richmond, A. D., and G. Lu (2000), Upper-atmospheric effects of magnetic storms: A brief tutorial, *J. Atmos. Sol. Terr. Phys.*, *62*, 1115–1127, doi:10.1016/S1364-6826(00)00094-8.
- Richmond, A. D., C. Peymirat, and R. G. Roble (2003), Long-lasting disturbances in the equatorial ionospheric electric field simulated with a coupled magnetosphere-ionosphere-thermosphere model, *J. Geophys. Res.*, *108*(A3), 1118, doi:10.1029/2002JA009758.
- Rishbeth, H. (1991), F-region storms and thermospheric dynamics, *J. Geomagn. Geoelectr.*, *43*, 513–524, doi:10.5636/jgg.43.Supplement1_513.
- Sastri, J. H., Sridharan, R. and Kumar Pant, T. (2003a) Equatorial ionosphere-thermosphere system during geomagnetic storms, in *Disturbances in Geospace: The Storm-Substorm Relationship*, edited by A. S. Sharma, Y. Kamide, and G. S. Lakhina, pp. 185–203, AGU, Washington, D. C., doi:10.1029/142GM16.
- Sastri, J. H., Y. Kamide, and K. Yumoto (2003b), Signatures for magnetospheric substorms in the geomagnetic field of dayside equatorial region: Origin of the ionospheric component, *J. Geophys. Res.*, *108*(A10), 1375, doi:10.1029/2003JA009962.
- Senior, C., and M. Blanc (1984), On the control of magnetospheric convection by the spatial distribution of ionospheric conductivities, *J. Geophys. Res.*, *89*, 261–284, doi:10.1029/JA089iA01p00261.
- Scherliess, L., and B. Fejer (1997), Storm time dependence of equatorial disturbance dynamo zonal electric fields, *J. Geophys. Res.*, *102*, 24,037–24,046, doi:10.1029/97JA02165.
- Seemala, G. K., and C. E. Valladeres (2011), Statistics of total electron content depletions observed over the South American continent for the year 2008, *Radio Sci.*, *46*, RS5019, doi:10.1029/2011RS004722.
- Somayajulu, V. V. (1998), Magnetosphere-ionosphere coupling, *Proc. Indian Natl. Sci. Acad.*, *64*(A3), 341–351.
- Spogli, L., et al. (2016), Formation of ionospheric irregularities over Southeast Asia during the 2015 St. Patrick's Day storm, *J. Geophys. Res. Space Physics*, *121*, 12,211–12,233, doi:10.1002/2016JA023222.
- Titheridge, J. E. (1995), Winds in the ionosphere—A review, *J. Atmos. Terr. Phys.*, *57*, 1681–1714, doi:10.1016/0021-9169(95)00091-F.
- Tsurutani, B. T., and W. D. Gonzalez (1997), The interplanetary causes of magnetic storms: A review, in *Magnetic Storms*, edited by B. T. Tsurutani, et al., pp. 77–89, AGU, Washington, D. C., doi:10.1029/GM098p0077.
- Tulasi Ram, S., P. V. S. Rama Rao, D. S. V. D. Prasad, K. Niranjana, S. Gopi Krishna, R. Sridharan, and S. Ravindran (2008), Local time dependent response of postsunset ESF during geomagnetic storms, *J. Geophys. Res.*, *113*, A07310, doi:10.1029/2007JA012922.
- Tulasi Ram, S., N. Balan, B. Veendhara, S. Gurubaran, S. Ravindran, T. Tsugawa, H. Liu, K. Niranjana, and T. Nagatsuma (2012), First observational evidence for opposite zonal electric fields in equatorial E and F region altitudes during a geomagnetic storm period, *J. Geophys. Res.*, *117*, A09318, doi:10.1029/2012JA018045.
- Tulasi Ram, S., et al. (2015), Duskside enhancement of equatorial zonal electric field response to convection electric fields during the St. Patrick's Day storm on 17 March 2015, *J. Geophys. Res. Space Physics*, *121*, 538–548, doi:10.1002/2015JA021932.
- Vasyliunas, V. M. (1970), Mathematical models of magnetospheric convection and its coupling to the ionosphere, in *Particles and Fields in the Magnetosphere*, edited by M. McCormac, pp. 60–71, Springer, New York, doi:10.1007/978-94-010-3284-1_6.
- Wolf, R. A. (1975), Ionosphere-magnetosphere coupling, *Space Sci. Rev.*, *17*, 537–562, doi:10.1007/BF00718584.
- Yizengaw, E., and M. B. Moldwin (2009), African Meridian B-field Education and Research (AMBER) array, *Earth Moon Planet*, *104*(1), 237–246, doi:10.1007/s11038-008-9287-2.
- Zhang, S.-R., P. J. Erickson, Y. Zhang, W. Wang, C. Huang, A. J. Coster, J. M. Holt, J. F. Foster, M. Sulzer, and R. Kerr (2017), Observations of ion-neutral coupling associated with strong electrodynamic disturbances during the 2015 St. Patrick's Day storm, *J. Geophys. Res. Space Physics*, *122*, 1314–1337, doi:10.1002/2016JA023307.